ELSEVIER

Journal of Chromatography A, 796 (1998) 3–14

JOURNAL OF CHROMATOGRAPHY A

Review

Refining the scale-up of chromatographic separations

F.G. Lode, A. Rosenfeld, Q.S. Yuan, T.W. Root, E.N. Lightfoot*

Department of Chemical Engineering, University of Wisconsin, Madison, WI 53706-1691, USA

Abstract

The use of heavily loaded columns and complex processing conditions makes scale-up of chromatographic separations a non-trivial process. The wide ranges of process conditions that must be investigated demands that a large number of preliminary experiments must usually be made in small columns and laboratory-scale work stations. These preliminary data can be biased by improper column packing, poor distributors and dispersion in auxiliary apparatus, and it is important to understand these disturbing factors in detail. Moreover, it is precisely at this macroscopic level that our understanding of the chromatographic process is weakest, for large columns as well as small. This paper addresses three of these factors: Efficient elimination of peripheral effects and characterization of both header flow distribution and packing non-uniformity. This will be done using a variety of experimental and analytical approaches including nuclear magnetic resonance imaging, computational fluid dynamics and mass transfer, and careful experimentation. © 1998 Elsevier Science B.V.

Keywords: Preparative chromatography; Flow distribution; Packing uniformity

Contents

1. Introduction

The goals of this discussion will be to characterize departures of column responses from expectations based on available idealized models of chromatographic dynamics, e.g. ref. [1]. We will be particularly concerned with eliminating the contributions of system peripherals to observed effluent curves and characterizing dispersion introduced by non-uniform distribution in headers and non-uniform column packing. These effects can be most effectively studied using small pulses of test solutes so that one stays in the region of linear equilibria and kinetics, but much information can also be gained under non-linear conditions if peripheral dispersion is concentrated downstream from the test column.

This task is facilitated by advances in modelling, as suggested in Fig. 1 and Tables 1–3. It is shown in Fig. 1 [1] that one can predict the behavior of well-designed commercial columns from the separate determination of key parameters such as distribution equilibria, intraparticle diffusivities and column void

*Corresponding author.

0021-9673/98/$19.00 © 1998 Elsevier Science B.V. All rights reserved.
PII S0021-9673(97)00872-8

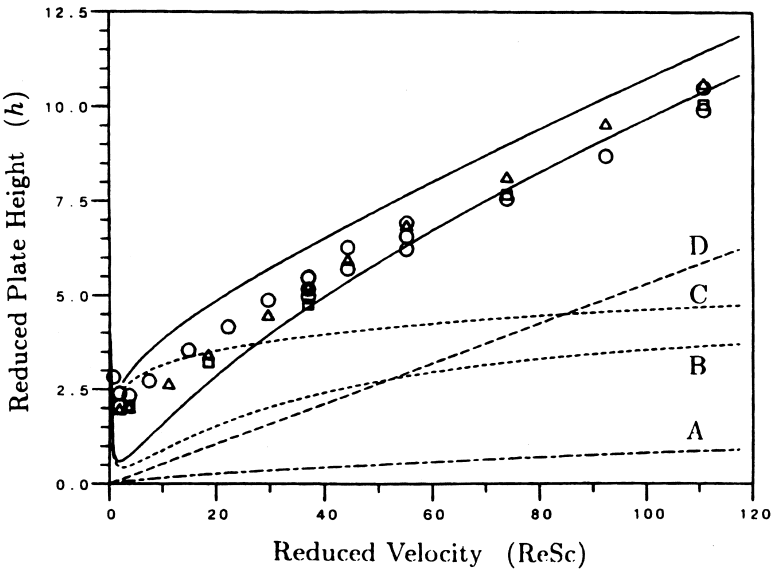

Fig. 1. Predictability of plate heights. The solid lines largely containing the data are the sums of prediction from available correlations for boundary layer resistance (A), convective dispersion bounds (B and C) and intraparticle diffusion. Data are for a commercial size exclusion column [1].

Table 1
Dimensional analysis at high space velocity

At high velocity and fast adsorption, a chromatographic column has only two time constants:

$$\bar{t} = V/Q = \frac{\pi}{4} D^2 L \cdot \frac{1}{\pi \epsilon_b D^2 v} \text{ and } T_{dif} \approx d_p^2/6D_{im}$$

It can thus be scaled simply by keeping the ratio:

$$\frac{LD_{im}}{v\varepsilon_b d_p^2} = \text{constant}$$

Table 2
Dimensional analysis of batch adsorption: Effect of column diameter (HyperD using BioSepra calculator)

$vd_p^2 \cdot 10^{-6}$	$d_p = 50$ μm			$d_p = 100$ μm		
	v	Capacity (%)	Pressure drop	v	Capacity (%)	Pressure drop
40				4000	64.0	136
10	4000	91.0	544	1000	91.0	34
5	2000	95.5	272	500	95.5	17
2.5	1000	97.8	136	250	97.8	8
1.25	500	98.9	68	125		
0.625	250	99.4	34			

Table 3
Dimensional analysis of batch adsorption: Effect of column length (HyperD and BioSepra calculator)

Length (cm)	Diameter (cm)	Velocity (cm/h)	Capacity (%)	Pressure
25	1	250	95.9	1
100	0.5	1000	96.3	8
400	0.25	4000	96.4	136
1600	0.125	16 000	96.4	2176

Table 4
Properties of temporal moments

Invariant:

$$M_0' = \int_{-\infty}^{\infty} c\,dt$$

Additive:

$$M_1' = \int_{-\infty}^{\infty} tc\,dt / M_0'$$

$$M_2 = \int_{-\infty}^{\infty} (t-\bar{t})^2 c\,dt / M_0'$$

$$\Rightarrow M_3 = \int_{-\infty}^{\infty} (t-\bar{t})^3 c\,dt / M_0' \Leftarrow$$

Note: $\bar{t} = M_1'/M_0'$

fraction. Table 1 [2], developed for rapid adsorption kinetics and short solute residence times, suggests that column behavior is determined, for any set of solute and sorbent, by the balance of two time constants, i.e. the solute mean residence time and the intraparticle diffusional response time. This suggestion, consistent with today's high percolation velocities, is demonstrated in Tables 2 and 3 for highly non-linear ion exchange [3]. The independence of particle diameter and column length is shown, respectively. These conclusions can be extended to slow adsorption by adding a time constant to characterize the adsorption rate. Moreover, the dimensional analysis of Table 1 can be extended to overloaded columns and gradient elution if one scales the loading volume and gradient strength with column volume, as defined by Yamamoto [4].

Departures from predicted behavior can normally be ascribed to some combination of the above non-idealities, and the task of the designer is to determine the extent and nature of the contributions from each. We now look at each of these sources of dispersion in turn.

2. Dispersion in system peripherals

This is normally the place to start, and peripherals are particularly suspect for small columns, such as those commonly used in work stations for process development. One can immediately estimate the importance of such dispersion qualitatively by comparing the observed effluent curves with those produced by the peripherals alone. However, obtaining the response of the column alone requires deconvolution, and accurate direct numerical results are very difficult to obtain. We therefore suggest that one proceeds by the method of moments, taking advantage of the additivity relations, justified by Lightfoot et al. [2] and Yuan et al. [5] and shown in Table 4. Additivity of the first absolute and the second central (variance) moments has long been familiar to chromatographers, and additivity of the third central moment has been justified recently [2,5]. These three moments and the mass balance provided by the zeroth moment suffice to characterize the mean residence time, effective system volume, dispersion about the mean and skewness. We show below by example that these three measures suffice for most purposes.

The first task is to determine these moments and, again, we find that direct numerical procedures are highly subject to error. This is especially true for the third moment and is primarily due to the importance

Table 5

$$\mathrm{DMG}(t) = \frac{A\sqrt{\bar{t}}\,\exp\{\bar{t}^2/\sigma^2\}}{\sqrt{8(c-a)}\sigma\tau}\, ie^{-ct} \cdot \left[\mathrm{e}^{-i\sqrt{b(c-a)}}\, erfc\left(\tfrac{1}{2}\sqrt{\frac{b}{t}} - i\sqrt{t(c-a)} \right) - \mathrm{e}^{i\sqrt{b(c-a)}}\, erfc\left(\tfrac{1}{2}\sqrt{\frac{b}{t}} + i\sqrt{t(c-a)} \right) \right]$$

where $a = \dfrac{\bar{t}}{2\sigma^2}$, $b = \dfrac{4\bar{t}^3}{2\sigma^2}$ and $c = \dfrac{1}{\tau}$

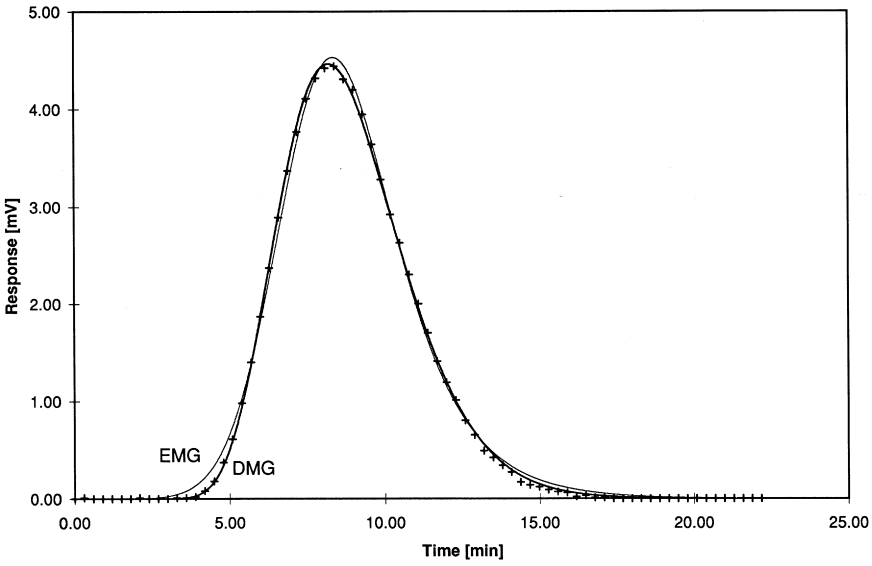

Fig. 2. Correlation of effluent concentration–time relations for lysozyme. The data (+) are compared with optimum fits for the DMG and EMG functions defined in the text [8].

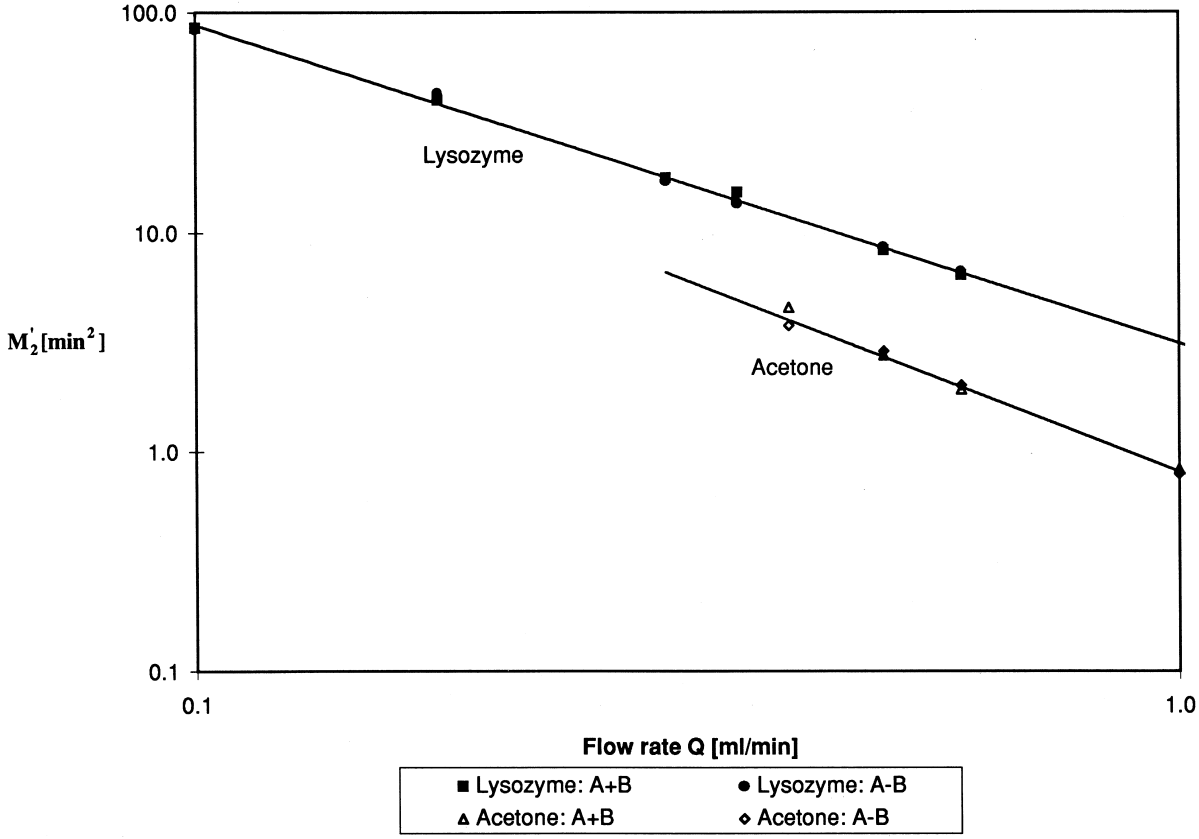

Fig. 3. Additivity test for the second central moments (variances). Comparisons of moments obtained from two techniques, i.e. summing the moments for two individual columns as measured separately (A+B) and moments measured for the two in series (A–B) are shown [8].

of long-time data (‘tails’ of the effluent curves) where the signal-to-noise ratio is high. This topic has already been extensively discussed in the analytical chemistry literature [6,7] and, for the first absolute and the second central moments, it has generally been satisfactory to use the exponentially modified Gaussian distribution, EMG, which is essentially the convolution of a Gaussian with an ideal mixer. However, we have found [8] that, for the third central moment, this is usually not satisfactory, and we have generated several fitting functions that must be tested for suitability in individual cases. We have found it useful to begin by using the modified Gaussian distribution

$$g_m(t) \equiv \frac{A}{\sigma\sqrt{2\pi t/\bar{t}}} \exp\left[-\frac{(t-\bar{t})^2}{2\sigma^2(t/\bar{t})} \right]$$

Here, t is the time at which the effluent appears, $\bar{t}$ is the mean solute residence time and σ^2 is the variance. This function describes the inherent skewness of effluent curves in ideal differential chromatography. Convolution of it with an ideal mixer produces the distribution function defined here as a ‘‘doubly modified Gaussian’’, DMG, and shown in Table 5. This function is frequently satisfactory and we illustrate its use below. In spite of its apparent complexity, the DMG is quite tractable numerically and always produces real values of concentration.

The use of the DMG is illustrated in Fig. 2 where it is compared with actual data for lysozyme in a 2.5-cm-long column with a 2-cm^2 cross-section packed with Sepharose big beads. The flow-rate was 0.5 ml/min and the protein was dissolved in a 1-*M* NaCl solution that was maintained at pH 6.8 with a sodium phosphate buffer. It has been used by us [8] for testing the feasibility of third moment additivity in actual practice. This was done by using two

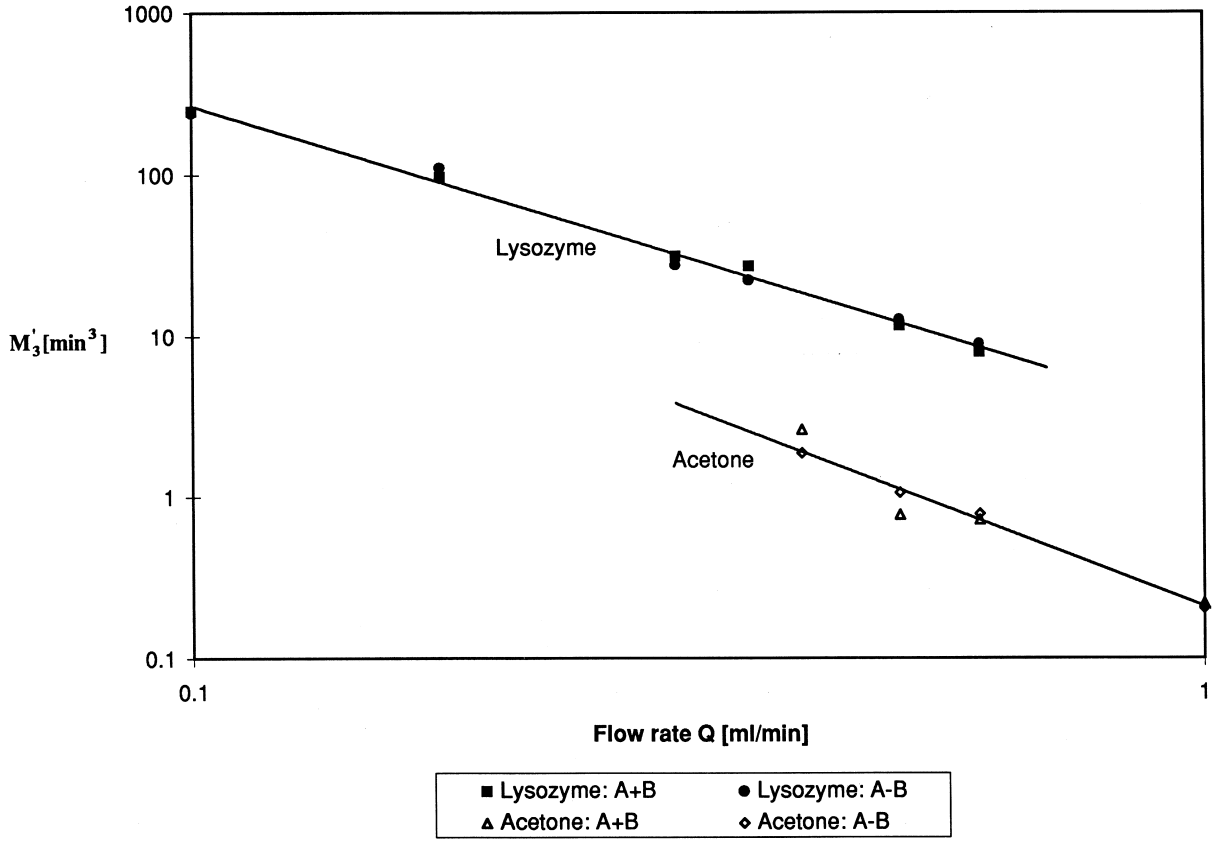

Fig. 4. Additivity test for the third central moments. Comparisons correspond to those in Fig. 3 [8].

columns, first operated singly and then in series, always with the same peripherals. The accuracy of the moment determinations can then be assessed by comparing the sums of component moments with that of the two in series (and subtracting the effects of the peripherals, which contribute strongly to the third central moment). The results obtained with lysozyme and acetone are shown in Figs. 3 and 4. The points labeled A+B represent the sums of the moments for the two columns, as measured separately, and points labeled A–B are the moments of the two columns in series. It may be seen that data scatter is somewhat larger for the third moment than for the second, but that useful estimates can be obtained in both cases. Moreover, there is no systematic difference in the results obtained by the two methods. It is our experience that calculated values of the higher moments are quite sensitive to noise in the original data. Careful attention to detail is necessary to obtain reproducible results. Baseline shifts usually cause catastrophic errors as it is almost impossible to correct adequately for these later.

3. Effects of intra-column non-idealities

Once peripheral effects have been eliminated, one can estimate the contributions of header maldistribution and non-uniform packing rather simply using the flow reversal technique of Roper and Lightfoot [9]. Here, one depends on the fact that all unavoidable physical sources of dispersion, intraparticle diffusion, boundary layer resistance and interparticle mixing, are microscopic: They occur on a length scale of packing diameter, and they are irreversible. Specifically, they are insensitive to the direction of flow.

The effects of header maldistribution and macroscopic packing non-uniformity, however, occur on length scales of column diameter and show the typical reversibility of all creeping flows. The recommended procedure then is to operate the column normally for a time equal to just half of the solute's mean residence time, then to reverse the direction of flow through the column and continue pumping at the original rate. The resulting effluent curve will be free of dispersion resulting from header non-ideality and the effects of macroscopically non-uniform packing to a surprisingly high level of accuracy .

The difference between the normal and flow-reversed effluent curves, examples of which are shown in Fig. 5 [5], then gives the dispersion caused by non-ideal header and packing. The flow reversed curve is less asymmetric than the conventional curve and has a smaller variance.

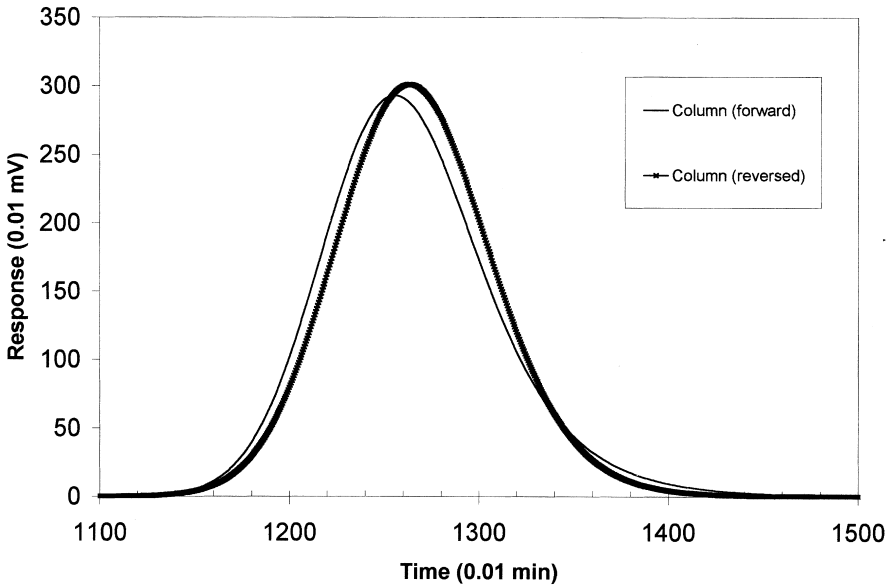

Fig. 5. Effect of flow reversal. Compared here is a normal effluent curve with one for the same column obtained from the flow reversal technique described in the text.

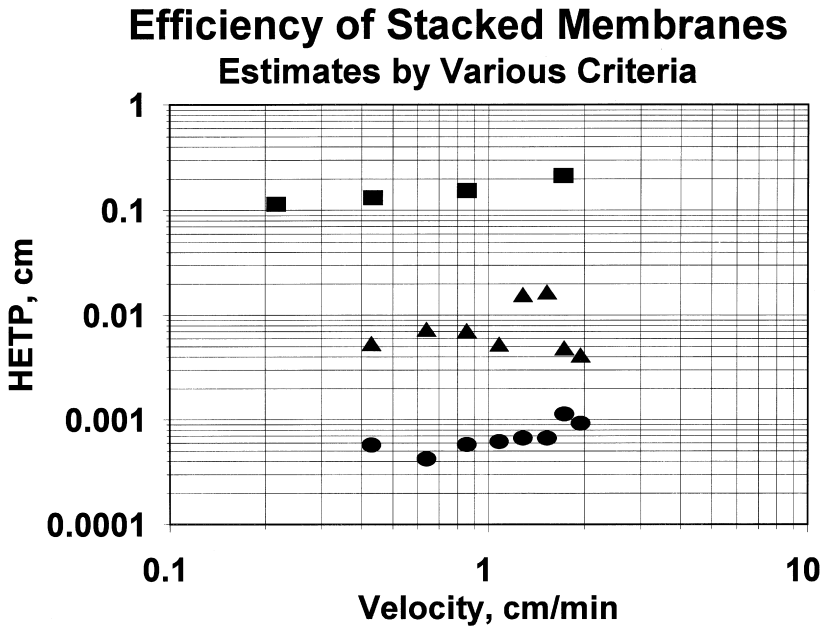

Fig. 6. Measures of plate height for a Millipore Memsep.

Another view of flow maldistribution is given in Fig. 6, where three different estimates of plate height are given for a small stacked-membrane chromatograph. The scaled plate heights $h=H/d_p$ for the middle group of points (triangles) are calculated directly from the variance according to the formula

$$h = H/d_p = (L/d_p)s^2/\bar{t}^2$$

where H is the plate height, d_p is the mean particle diameter, L is the length of the column, s^2 is the variance of the entire effluent curve and $\bar{t}$ is the solute's mean residence time. The lower set (circles) is calculated from the estimated local variances, eliminating the effects of flow maldistribution. The upper set (squares) was calculated by Yamamoto and Sano [10] from non-linear frontal analysis, assuming a constant-form front. The very high estimated plate heights from this upper set probably result from the failure of the one-dimensional model used: For macroscopically non-uniform flows, band width does not approach an asymptotic value but actually increases linearly with time. Confirmation of the suspected maldistribution is shown in Fig. 7 [2], where nuclear magnetic resonance (NMR) flow imaging shows that there is a marked variation in percolation velocity over the cross-section investigated.

Flow maldistribution can result from faulty header design, and this is quite likely for the system of Fig. 7, but, to date, this problem has not received much systematic attention. Since flow is for the most part laminar, it is possible to simulate header flow via computational fluid dynamics. One such example is illustrated in Fig. 8, for a differential solute feed

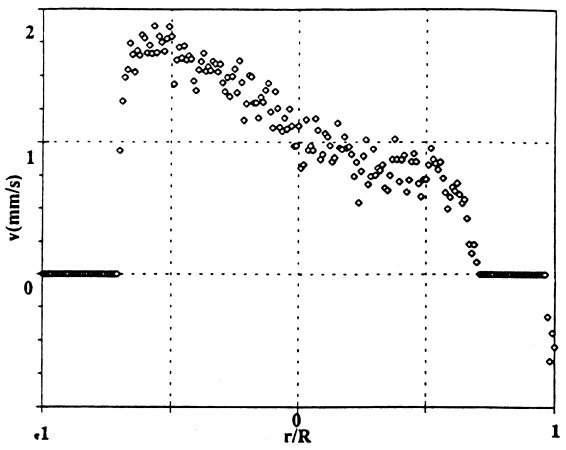

Fig. 7. Velocity distribution over the diameter of a Memsep. Data taken by nuclear magnetic resonance flow imaging by Roper [20].

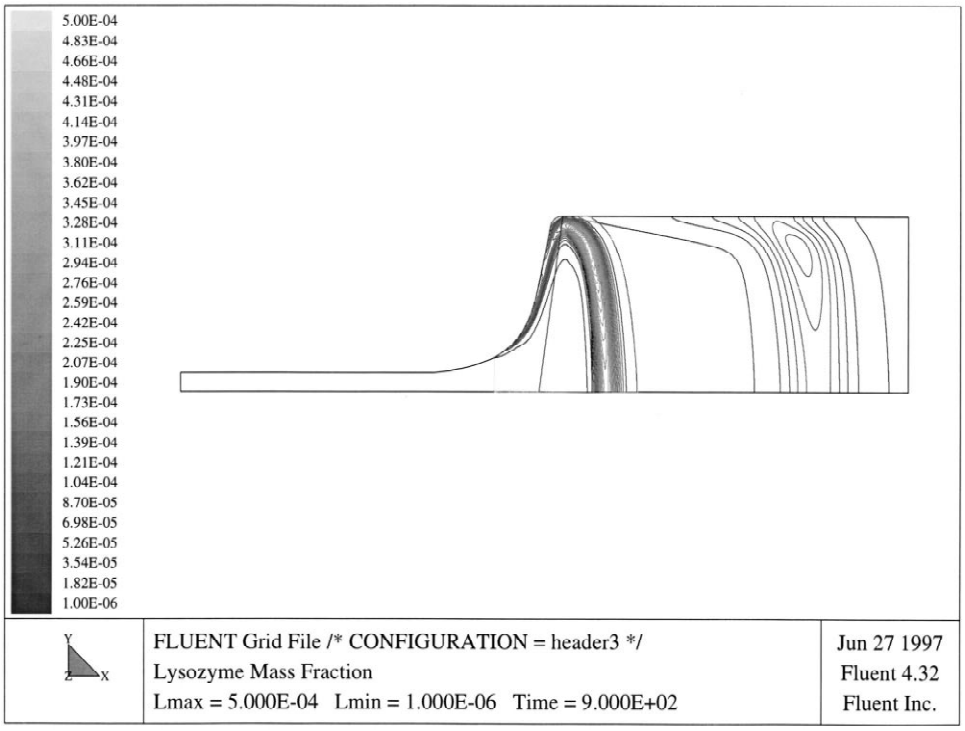

Fig. 8. Simulated concentration distributions for a novel header connected to a uniform packed bed. Shown are results for two different times.

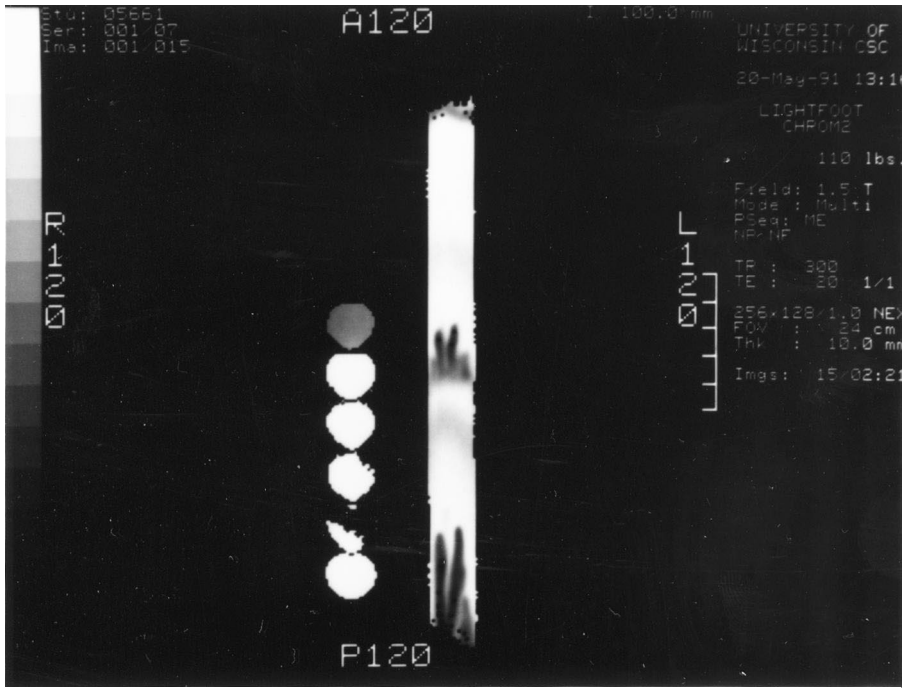

Fig. 9. Viscous fingering induced by viscosity gradients. From Athalye [21].

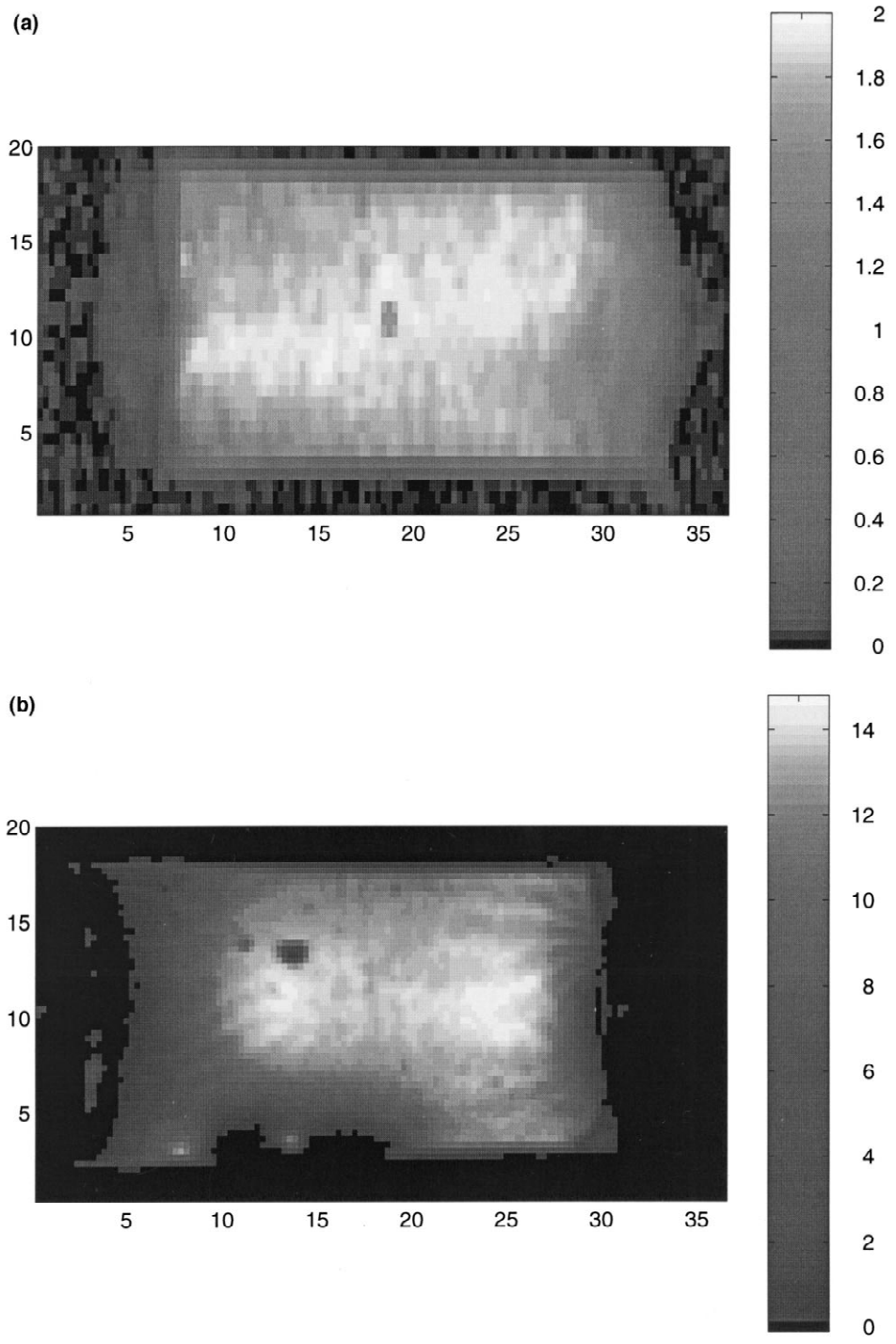

Fig. 10. Proton distributions in a packed column (a) and NMR spin echo images (b) [14].

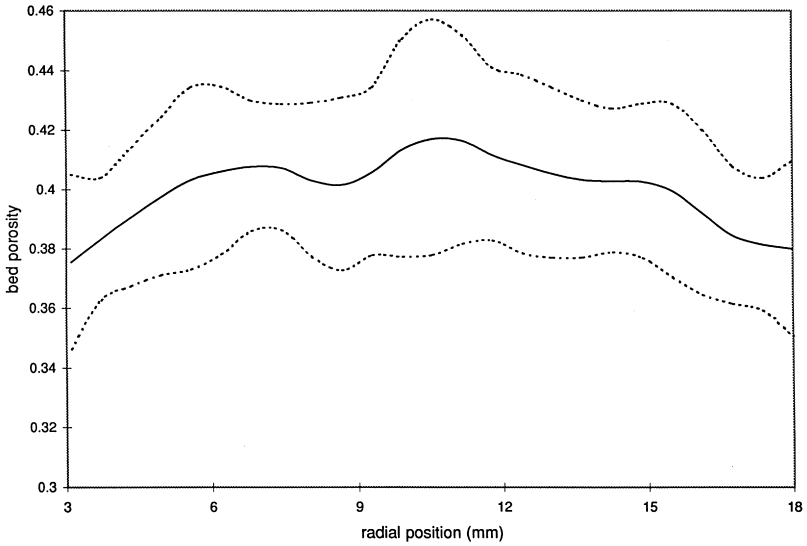

Fig. 11. Average radial proton distribution for the column of Fig. 10a [14]. The dotted lines are error limits.

pulse. Here, the contours represent lines of constant concentration, calculated for solution diffusion as the only source of microscopic dispersion. It may be seen that the solute distribution is fairly sharp in the axial direction but shows quite significant radial variation. For such a distribution, local overloading will occur before area average concentrations are high, and the radial non-uniform viscosity resulting from this solute distribution could, in turn, trigger the kind of hydrodynamic instability shown in Fig. 9 [13]. Note that the size scale of the fingers corresponds closely to the scale of solute non-uniformity in Fig. 8.

Significant packing non-uniformity is especially common in the small columns often used with work stations, and an example is shown in Fig. 10a. Here, proton concentration is given by a spin echo imaging process, and a higher void fraction is found in the

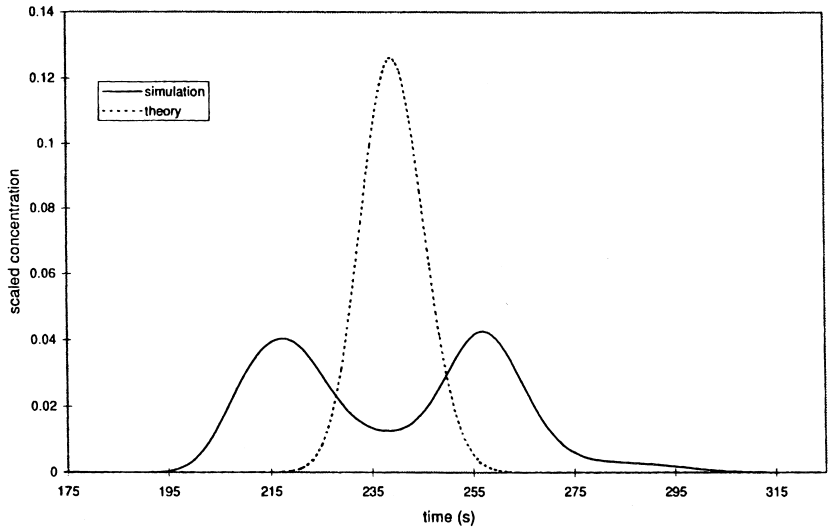

Fig. 12. Simulated effluent curves for the system of Fig. 10a [14].

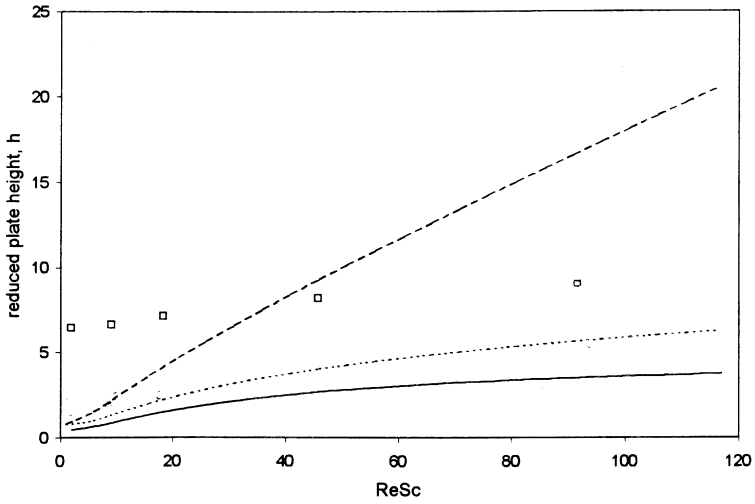

Fig. 13. Predicted van Deemter plot for the system of Fig. 10a [14].

central region of the column. The local void fraction may be calculated from proton density, and this approach is used to produce Fig. 11, where the estimated radial distribution averaged over the column length is shown.

One can now estimate local percolation velocities from the Blake-Kozeny equation and construct streamlines. This was done [14] here using the computational fluid dynamic simulation program, FLUENT (Fluent, Lebanon, NH, USA) for non-adsorbing spheres. The distribution of solute hold-up times was estimated, using the axial dispersion correlation of Gunn [11,12] for the diffusion coefficient in the FLUENT program. This approach predicts a double peaked curve, as shown in Fig. 12, for the column of Fig. 10a, compared with the corresponding prediction for uniform percolation velocity. The result is sharply reduced separability where axial dispersion dominates, and a corresponding upper limit on numbers of plates: Plate heights are the sum of contributions from the various dispersion-inducing mechanisms. However, at high percolation velocity, internal diffusion tends to increasingly dominate over dispersion in reducing the total plate number and, above some transition velocity, the degree of packing uniformity shown here may not be serious. This is suggested by the van Deemter plot of Fig. 13, where the effects of axial dispersion and intraparticle diffusion are compared.

Many small columns show worse non-uniformities than that of Fig. 10a, and one such example, which is not atypical, is illustrated in Fig. 10b [13]. Here, there is a significant air bubble along with other serious, but less drastic, density variations.

It should be noted, however, that the spin echo technique tends to exaggerate the size of bubbles and also that it is being pushed towards its limits in this application. A discussion of NMR imaging in this context is provided elsewhere [14,15].

4. Comparison with other systems

Much work remains to be done to evaluate non-idealities in header design and packing techniques, and the first requirement is for better measurement. NMR imaging is promising for small columns, but, even here, artifacts resulting from sudden susceptibility changes as well as field perturbations present formidable challenges. It may prove desirable to adapt techniques used in evaluating non-uniformity in ceramics and metallic composites [16–18] as well as pharmaceutical tabletting [19], where similar problems are encountered. It will also be highly desirable to start rheological modelling of column-packing processes, and here also, the ceramic and powder metallurgy literature may prove useful. These points will be discussed elsewhere.

References

[1] A.M. Athalye, S.J. Gibbs, E.N. Lightfoot, J. Chromatogr. 589 (1992) 71–85.
[2] E.N. Lightfoot, J.L. Coffman, F. Lode, Q.S. Yuan, T.W. Root, J. Chromatogr. A 760 (1997) 139–149.
[3] BioSepra, Inc., Simulation program for calculating chromatographic column performance for protein separations.
[4] S. Yamamoto, Biotech. Bioeng. 48 (1995) 444–451.
[5] Q.S. Yuan et al., in preparation.
[6] J.P. Foley, J.G. Dorsey, Anal. Chem. 55 (1983) 730–737.
[7] M.S. Jeansonne, J.P. Foley, J. Chromatogr. 459 (1992) 65–77.
[8] A. Rosenfeld et al., in preparation.
[9] D.K. Roper, E.N. Lightfoot, J. Chromatogr. A 702 (1995) 69–80.
[10] S. Yamamoto, Y. Sano, J. Chromatogr. 597 (1992) 173–179.
[11] D.J. Gunn, Trans. Inst. Chem. Eng. 47 (1969) T351–T359.
[12] D.J. Gunn, Chem. Eng. Sci. 42 (1987) 363–373.
[13] E.N. Lightfoot, A.M. Athalye, J.L. Coffman, D.K. Roper, T.W. Root, J. Chromatogr. A 707 (1995) 45–55.
[14] F. Lode, M.Sc. Thesis, University of Wisconsin, 1997.
[15] F. Lode and T.W. Root, in preparation.
[16] T.A. Ring, Fundamentals of Powder Processing and Synthesis, Academic Press, 1996.
[17] B.-B. Hwang, S. Kobayashi, Int. J. Mach. Tools Manufact. 31 (1991) 123–137.
[18] R.A. Thompson, Am. Ceramic Soc. Bull. 60 (1981) 237–243.
[19] D. Train, Trans. Inst. Chem. Eng. 35 (1957) 258.
[20] D.K. Roper, Ph.D. Thesis, University of Wisconsin, 1994.
[21] A. Athalye, Ph.D. Thesis, University of Wisconsin, 1993.